TABLE OF CONTENTS

Section Page

SECTION 1
BEAM NORMAL SINGLE SPIN ASYMMETRY

1.1 Introduction

Dedicated measurements of the beam normal single spin asymmetry in inelastic e+p, and e+N scattering with $\Delta(1232)$ in the final state were performed during 18th - 20th February 2012 at Hall-C of Jefferson Lab using Q-weak apparatus.

1.2 Experimental Method

The Q-weak longitudinal measurement setup [1] was used for inelastic transverse measurement. The electron beam polarization was changed from nominal longitudinal setup to produce fully horizontal/ vertical polarization using the double Wien filter at the injector (Section **??**). Torodial magnet setting was changed to 6700 A (nominal magnet current for elastic running was 8901 A) to focus inelastically scattered electron into the main Čerenkov detector.

1.2.1 Available Data Set and Condition of Experimental Data Taking

Total collected data after hardware and software quality checks is shown in Table 1.1. The QTor current of 6700 A selects the inelastic events in the e+P and e+N scattering. Data on both sides of the inelastic peak (6000 A and 7300 A) were taken to improve simulation of elastic dilution. Two transverse spin orientations, horizontal and vertical, were used to study the asymmetry cancellation between the opposite octants (octants 3 & 7 and 1 & 5 for horizontal and vertical respectively) of the Čerenkov detectors. Data were collected on liquid hydrogen (LH_2) cell, 4% thick downstream aluminum alloy (Al), and a 1.6% thick downstream carbon foil (^{12}C) with 1.155 GeV beam for both spin orientations (as shown in Table 1.1). Different beam currents (I) were used on different targets, as shown in Table 1.1. The beam was rastered on the target over an area of 4 mm$\times$4 mm by the fast raster system to minimize the target boiling. The Insertable Half Wave Plate (IHWP) was used to remove further helicity correlated beam asymmetries and was reversed at intervals of about 2 hours. More information about the condition of data taking is given in APPENDIX-**??** section **??**.

Table 1.1 Transverse N-to-Δ data set. The data set for vertical transverse polarization are in parentheses, rest are from horizontal transverse polarization. The beam current for different targets are shown in second last row. Amount of transverse data collected in terms of the total charge in Coulombs are shown in bottom row.

IHWP	QTor current					
	6000 A	6700 A			7300 A	
	LH_2	$LH_2^{\dagger}$	$Al^{\dagger\dagger}$	^{12}C	LH_2	Al
IN	16152 16153	(16066) 16131 16132	(16067) 16115 16116	16150 16151	16133 16134 16135	16122 16123 16124 16160
OUT	16154 16156 16157 16158	(16065) 16129 16130	(16068) (16069) 16117 16118 16119	16148 16149	16136 16137	16120 16121 16161
Beam current I [μA]	180	180	60	75	180	60
Collected Data [C]	1.5	1.8 (1.9)	0.8(0.4)	0.6	2.0	0.9

In this dissertation, full analysis of the beam normal single spin asymmetry from inelastic electron-proton scattering on LH_2 target, indicated by † in Table 1.1, will be discussed. The transverse asymmetry on Al target, indicated by †† in the table, was also analyzed as a background correction for the LH_2 target. The analysis of the remaining data are ongoing and will not be covered in this dissertation.

1.3 Extraction of Raw Asymmetries

Single detector asymmetry was obtained by averaging two PMT asymmetries of the Čerenkov detector. The error weighted average of the asymmetries from runlets, ∼5 minutes long data samples, was extracted as the average asymmetry for a given data set. To extract the uncorrected raw asymmetry A_{raw} from the detectors, the average asymmetry for the two different Insertable Half Wave Plate (IHWP) settings, IN and OUT, were determined separately for each main detector bar. The asymmetries measured in the IHWP configurations were sign corrected for the extra spin flip and averaged together after checking for the IHWP cancellation of the false asymmetries. The error weighted value of IN-OUT yields the measured raw asymmetry for each bar. These raw asymmetries were then plotted against the detector octant number, which represents the location of the detector in the azimuthal plane (ϕ = (octant - 1)×45°), and they were fitted using a function of the form

in Equation 1.3.1. The transverse asymmetries show azimuthal modulation behavior, hence this analysis will focus on the azimuthal dependence of the detector asymmetries.

$$f(\phi) = \begin{cases} \text{Horizontal transverse: } A_M^H \sin(\phi + \phi_0^H) + C^H \\ \text{Vertical transverse: } A_M^V \cos(\phi + \phi_0^V) + C^V \end{cases} \tag{1.3.1}$$

Here, ϕ is the azimuthal angle in the transverse plane to the beam direction. $\phi = 0$ indicates beam left, ϕ_0 is the constant phase offset in ϕ, A_M is the measured asymmetry (amplitude) of the azimuthal modulation generated by BNSSA, and C is a constant appearing for monopole asymmetries such as the parity violating asymmetry generated by residual longitudinal polarization in the beam. The measured un-regressed raw asymmetries for the horizontal and vertical transverse polarization on LH_2 target are $A_{raw}^H = 5.34 \pm 0.53$ ppm and $A_{raw}^V = 4.60 \pm 0.81$ ppm respectively.

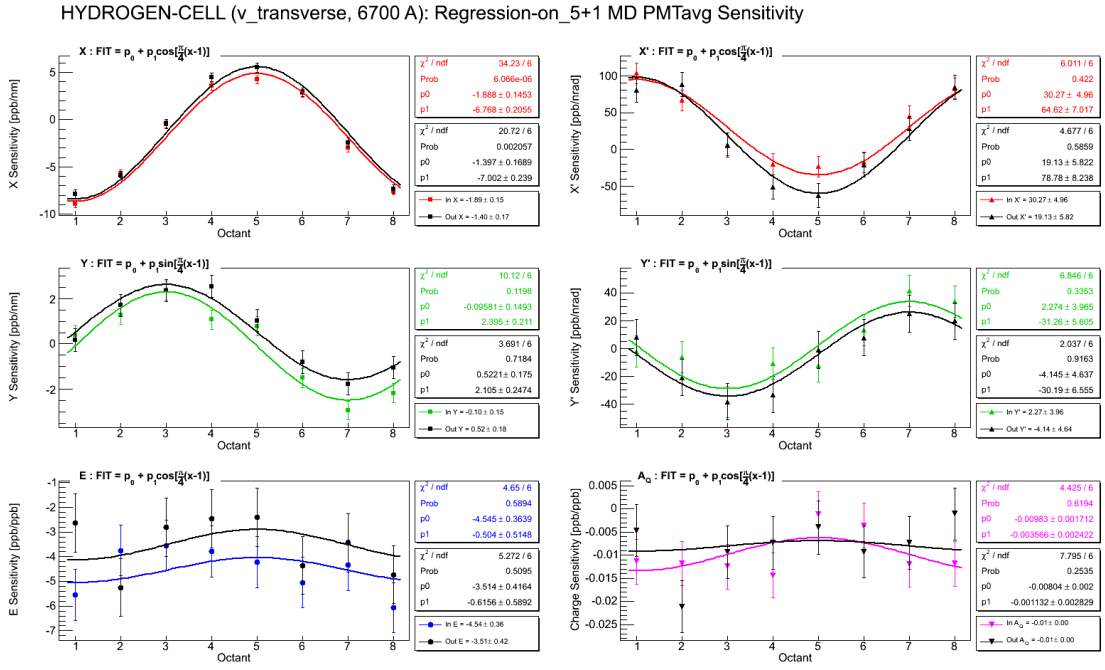

Figure 1.1 Azimuthal dependence of the main detector sensitivities to HCBA with respect to 5+1 regression scheme in the vertical LH_2 transverse data set are shown here. Beam positions and angles have sinusoidal dependence with octant. No such dependence is seen for energy and charge. Two IHWP states are shown separately for each beam parameter. Fit functions used to fit the parameters are shown on the plot. The constant in the fit gives the error weighted average of the sensitivities. See APPENDIX-??, section ?? for the sensitivities and corrections from full data sets.

1.4 Asymmetry Correction using Linear Regression

The helicity correlated changes in the electron beam position, angle, and energy change the effective scattered angle and energy of the electrons in the detector acceptance. Changes in these beam parameters can create false asymmetry in the detector and need to be corrected before the extraction of the physics asymmetry. A multi variable linear regression [2] is used to remove the beam asymmetries from the raw Čerenkov detector asymmetries as shown in Equation 1.4.1.

$$A_M = A_{raw} - \sum_{i=1}^{6} \left(\frac{\partial A_{raw}}{\partial T_i} \right) \Delta T_i \tag{1.4.1}$$

Here A_M is the measured asymmetry after regression, and $(\partial A_{raw}/\partial T_i)$ is the detector sensitivity to a helicity-correlated beam parameter T_i with differences ΔT_i. During this measurement period, the helicity-correlated differences were stable (shown in Figure **??**, and **??**) and are summarized in Table 1.2. The detector sensitivity slopes are calculated with linear regression, which uses natural beam motion during a runlet and considers correlations between different beam parameters. The asymmetries presented in this dissertation are regressed against six (5+1) beam parameters (T_i): horizontal position (X), horizontal angle (X'), vertical position (Y), vertical angle (Y'), the energy asymmetry (A_E), and the charge asymmetry (A_Q). Regression assumes a linear correlation between each variable. The sensitivities of the Čerenkov detectors to different helicity correlated beam parameters have azimuthal dependence, as shown in Figure 1.1 (shown for vertical transverse data only, horizontal transverse can be found in Figure **??**). This azimuthal dependence of the position and angle sensitivities are a result of the movement of the scattered electron profile across the octants which changes the effective scattering angle of the detected electrons not specific to the transverse asymmetry measurement. The position and angle sensitivities are anti-correlated. The energy and charge sensitivities are not expected to have any azimuthal dependence since they do not change the acceptance. The size of the applied correction to the raw asymmetries depends on the size of the helicity-correlated beam parameter differences ΔT_i and the sensitivities $(\partial A_{raw}/\partial T_i)$. The size of the corrections were ∼2-3 order of magnitude smaller compared to the size of the measured asymmetry and are shown in Figure 1.2 (shown for vertical transverse data only, horizontal transverse can be found in Figure **??**). The total applied regression correction (Figure 1.3) is dominated by the X correction (Figure 1.2 top left).

The regressed (5+1) asymmetries measured using horizontal and vertical transverse polarization beam on LH_2 target are shown in Figure 1.4. The azimuthal modulating asymmetry flips sign with

Table 1.2 Beam parameter differences during for the horizontal and vertical transverse data set. The X differences are higher compared to Y differences.

Beam parameter differences	Horizontal		Vertical	
	IHWP IN	IHWP OUT	IHWP IN	IHWP OUT
ΔX [nm]	23.8 ± 2.1	20.6 ± 2.3	15.4 ± 3.1	58.0 ± 3.6
ΔY [nm]	6.9 ± 2.1	5.6 ± 2.3	20.2 ± 3.1	15.4 ± 3.6
ΔX′ [nrad]	0.7 ± 0.1	0.7 ± 0.1	0.6 ± 0.2	1.3 ± 0.2
ΔY′ [nrad]	0.2 ± 0.1	-0.3 ± 0.1	0.6 ± 0.2	0.9 ± 0.2
ΔE [ppb]	-2.3 ± 2.1	-1.5 ± 2.3	0.5 ± 3.1	-5.4 ± 3.6
ΔA_Q [ppb]	8.2 ± 0.5	-237.3 ± 55.6	60.1 ± 0.7	158.1 ± 88.1

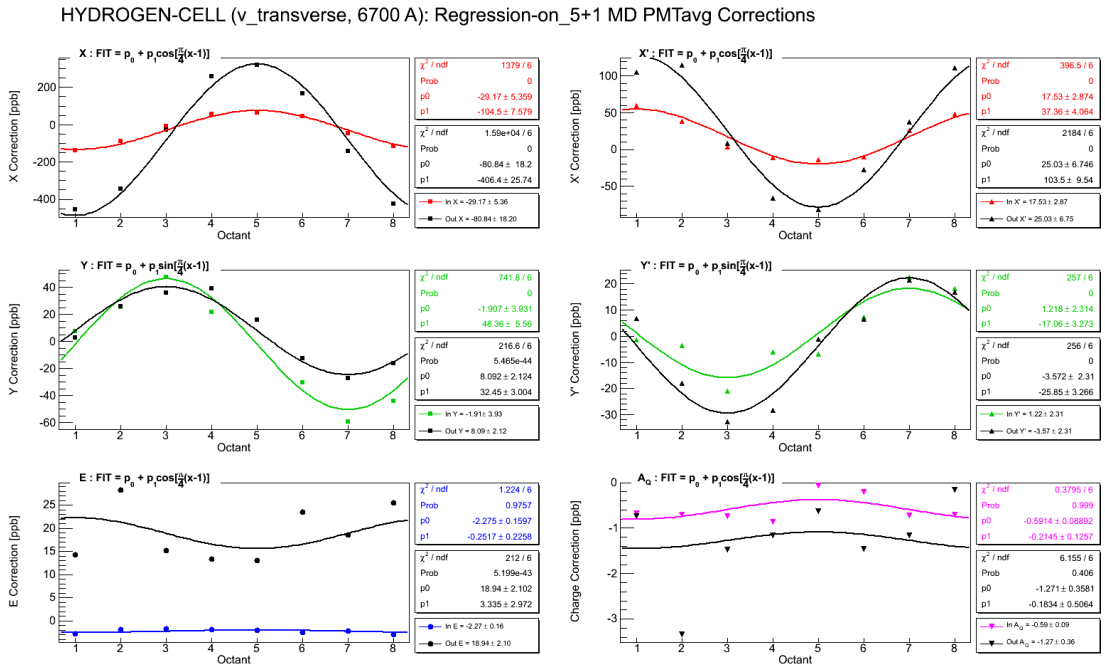

Figure 1.2 Main detector corrections (using sensitivities and differences from 5+1 regression scheme) vs octant for vertical LH_2 transverse data set are shown here. Beam positions and angles have sinusoidal dependence with octant inherited from the sensitivities. No such dependence is seen for energy and charge. Two IHWP states are shown separately for each beam parameter.

the insertion of the IHWP as expected. The vertical transverse asymmetries may show sign of phase shift between IHWP IN and IHWP OUT settings, but may be explained due to statistical fluctuation. Transverse polarization angle was ∼3-4° off from ideal settings during the measurement, which can not be confirmed with the statistics in hand. The (IN+OUT)/2 given by the $C^{(IN+OUT)/2}$ are compatible with zero within the measurement uncertainties. This null asymmetry indicates

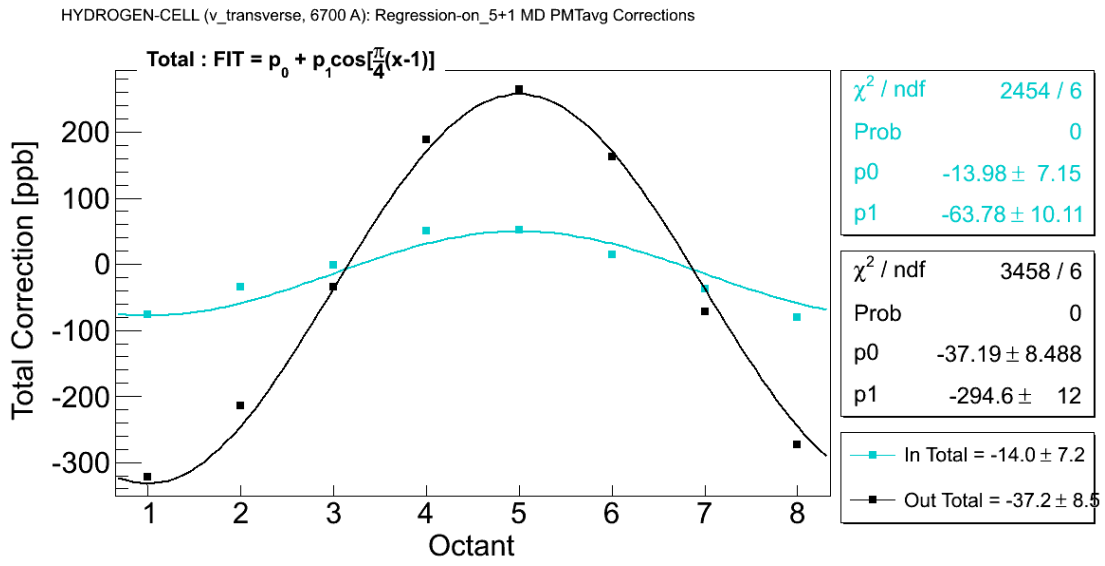

Figure 1.3 Total corrections (using sensitivities and differences from 5+1 regression scheme) vs octant for vertical transverse data set are shown here. Total correction is the sum of all the corrections (with sign) shown in Figure 1.2.

the azimuthal modulating component in both IHWP IN and OUT are analogous, and the non-polarization dependent false beam asymmetries were successfully removed by the regression.

The error weighted value of IN-OUT yields the measured regressed asymmetry for each bar. As expected from the azimuthal dependence of the BNSSA, there is a 90° phase offset between the two modulations, as shown in Figure 1.5. The measured regressed asymmetries using horizontal and vertical transverse polarization are extracted as $A_M^H = 5.34 \pm 0.53$ ppm and $A_M^V = 4.53 \pm 0.81$ ppm respectively. The combined (error weighted average) regressed asymmetry from horizontal and vertical transverse polarization is given by

$$A_M = 5.095 \ \pm \ 0.444 \text{ ppm (stat)}. \tag{1.4.2}$$

This measurement provides a ∼9% statistical measurement of the BNSSA in inelastic e+p scattering (not corrected for backgrounds, polarization or other experimental related systematic uncertainties). Regression has minimal effect on the extracted measured asymmetries as the corrections are too small compared to the size of the asymmetries.

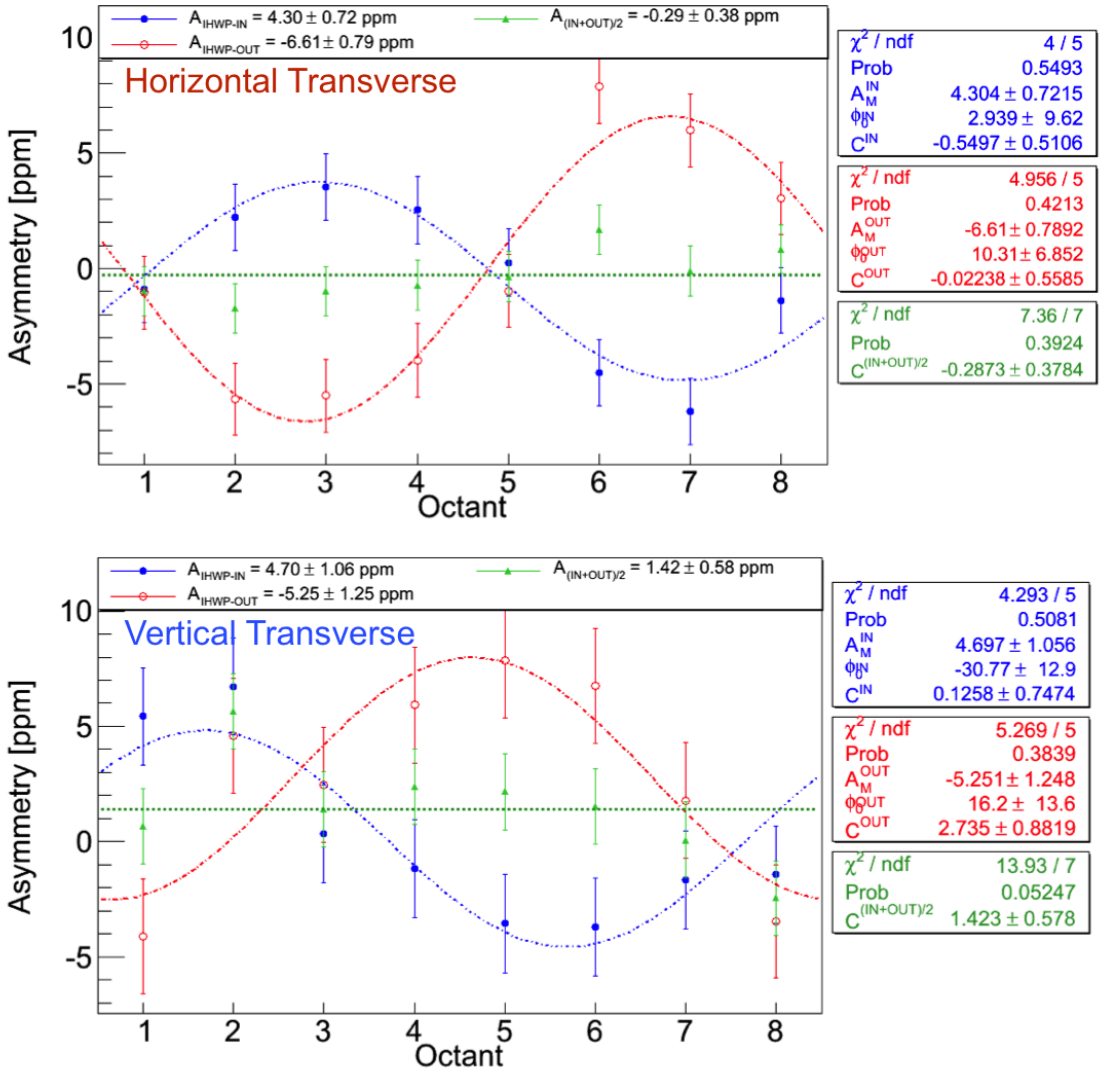

Figure 1.4 Main detector asymmetry for horizontal (top), vertical (bottom) transverse data set. For comparison, asymmetries for IN and OUT data are also shown separately. The regressed asymmetries change sign with the insertion of the IHWP with comparable amplitudes due to spin dependence. The (IN+OUT)/2 asymmetries of the eight Čerenkov detectors, given by $C^{(\mathrm{In+Out})/2}$ is compatible with zero except in the vertical data set. The extraction of BNSSA depends on the amplitudes in the fits and by comparison of IN and OUT, not the constant term.

1.4.1 Azimuthal Acceptance Correction

The acceptance of a single Q-weak Čerenkov detector is only 49% of an octant (section **??**). So the reported asymmetry from a detector is an average over 22° azimuthal angle (ϕ). Each detector bar measures an average asymmetry over a range of ϕ selected by the collimators about its nominal

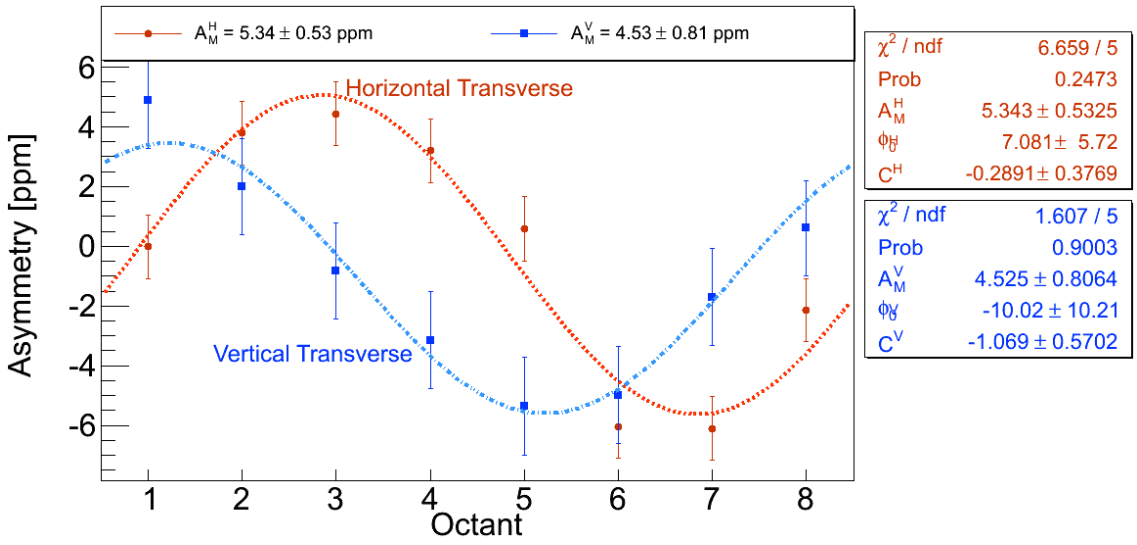

Figure 1.5 Regressed main detector asymmetry for horizontal, vertical transverse polarization are shown with red circle and blue square respectively. Data points for horizontal transverse are ∼4 hour long measurement, whereas vertical transverse data points are ∼2 hour long. The fit functions used are $A_M^H \sin(\phi + \phi_0^H) + C^H$ for horizontal transverse and $A_M^V \cos(\phi + \phi_0^V) + C^V$ for vertical transverse respectively. Asymmetries in each case shows ∼90° phase offset, as expected between horizontal and vertical configurations.

location (details in [3]). The effect of averaging cosines for a variable of the form $y(\phi) = A\cos(\phi+\delta)$ over the azimuthal angle yields

$$AVG[y(\phi)] = \frac{A\int_{\phi_0-\Delta\phi}^{\phi_0+\Delta\phi}\cos(\phi+\delta)\,\mathrm{d}\phi}{(\phi_0+\Delta\phi)-(\phi_0-\Delta\phi)} = A\cos(\phi_0+\delta)\times\frac{\sin\Delta\phi}{\Delta\phi}, \tag{1.4.3}$$

where ϕ_0 is the nominal azimuthal location of the detector with $\Delta\phi$ coverage. Similarly, for sines, $AVG[y(\phi)] = A\sin(\phi_0+\delta)\times\frac{\sin\Delta\phi}{\Delta\phi}$. So the measured asymmetry from each detector needs to be scaled by a factor of $\frac{\sin\Delta\phi}{\Delta\phi}$ to correct for the acceptance. A sinusoidal function was used to extract the transverse asymmetry due to azimuthal dependence of the measured asymmetry. So it was important to correct for the detector azimuthal acceptance. Assuming the collimator removes 49% of the octant acceptance (i.e 49% of 45°), $\Delta\phi = 11.025°$ yields the scale factor to be $\frac{\sin\Delta\phi}{\Delta\phi} = 0.9938$. The detector acceptance corrected measured asymmetry can be extracted as

$$A_M^{in} = 5.127 \text{ ppm}. \tag{1.4.4}$$

A conservative 50% uncertainty was used for $\Delta\phi$, which yields a systematic uncertainty of 0.004 in the correction.

1.5 Systematic Uncertainties

The dominant uncertainty in the measured asymmetry for this measurement is statistical (9%). A preliminary treatment of the systematic uncertainty performed on the data set is presented in this section.

1.5.1 Regression Scheme Dependence

The 5+1 linear regression scheme considered for this analysis is one of the many different schemes available and was worth investigating the regression corrections from several choices for the regression basis. A list of all the independent variables for different regression sets are shown in APPENDIX-**??**. Ideally, the regression results from all the schemes should agree if all equipment is functioning properly and the regression is being done properly. The differences in the regressed asymmetries can arise from differences in the noise, resolution, and non-linear response of the monitors. To compare for the systematic studies, a common set of event cuts [4] are applied to all regression schemes to match the quartets used by each scheme.

Table 1.3 Asymmetries from different regression scheme along with un-regressed asymmetry are shown for horizontal and vertical transverse data set from Run 2 Pass 5 database. Correction (difference between regressed and un-regressed asymmetry) on measured main detector transverse asymmetry due to regression schemes are small compared to the amplitude of the measured asymmetry. Set 5 and 6 were not available due to failure of BPM 9b during Run 2. Set 9 was ignored for this analysis as it contains the upstream luminosity monitor, which is not an independent variable (mainly used for diagnostic purpose), as one of the regression variable (more details about regression variables are in APPENDIX-**??**).

Regression scheme	Horizontal		Vertical	
	Asymmetry [ppm]	Correction [ppm]	Asymmetry [ppm]	Correction [ppm]
UnReg	5.339	0.000	4.602	0.000
std	5.343	0.004	4.524	-0.078
5+1	5.343	0.004	4.525	-0.077
set3	5.343	0.004	4.525	-0.077
set4	5.343	0.004	4.527	-0.076
set7	5.347	0.007	4.529	-0.073
set8	5.346	0.007	4.531	-0.072
~~set9~~	~~5.343~~	~~0.003~~	~~4.534~~	~~-0.069~~
set10	5.343	0.003	4.526	-0.077
set11	5.343	0.004	4.524	-0.078
Max - Min	set8 - set10	0.004	set8 - set11	0.006

Measured main detector asymmetries depends on choice of regression schemes and are summarized in Table 1.3. The regression scheme dependent uncertainty is defined as the largest difference

between all of the schemes and estimated to be 0.004 ppm for horizontal transverse and 0.006 ppm for vertical transverse data set.

1.5.2 Regression Time Dependence

The standard regression algorithm works with 5 minute runlet averaged quantities. The detector sensitivities are averaged over each runlet and corresponding differences are used to correct for the false asymmetry for each quartet in the runlet. There is another systematic uncertainty associated with regression time period that is considered. The effect of using slug, few hours, as time period for the regression instead of runlets was determined. The error weighted average sensitivities for a slug were calculated and average beam parameter differences for that slug were used to get the corrections, as shown in Equation 1.5.2. These slug averaged corrections were then used to regress asymmetries (Equation 1.5.1).

$$\langle A_{reg}\rangle_{slug} = \langle A_{UnReg}\rangle_{slug} - \langle C\rangle_{slug} \tag{1.5.1}$$

$$\langle C\rangle_{slug} = \sum_{i=1}^{6} \left\langle \frac{\partial A}{\partial T_i} \right\rangle_{slug} \langle \Delta T_i\rangle_{slug} \tag{1.5.2}$$

where T_i's are X, X', Y, X', A_E, and A_Q. The slug averaged sensitivities and beam parameter differences for the data set are shown in Figure 1.1 (also Figure **??** for horizontal transverse) and Table 1.2 respectively. The impact on regressed asymmetries due to change in the regression averaging time period for horizontal and vertical transverse data set are 0.006 ppm and 0.008 ppm respectively and are assigned as regression time dependence systematic uncertainties. More details in APPENDIX-**??** section **??**.

1.5.3 Nonlinearity

The Čerenkov detector signals are normalized to the charge and the charge asymmetry is actively driven to zero using a charge feedback system. The nonlinearity of the BCM electronics, the main detector electronics and target density fluctuations can induce nonlinear distortions in the charge asymmetry and hence in the measured asymmetry [5]. This nonlinearity of the system is seen to be non-zero from the non-zero constant term in the (5+1) regressed detector asymmetries, as shown in Figure 1.6. For both horizontal and vertical polarization data sets, nonlinearity is found to be -1%. At present, no proper method of handling the measured asymmetry distortion due to nonlinearity

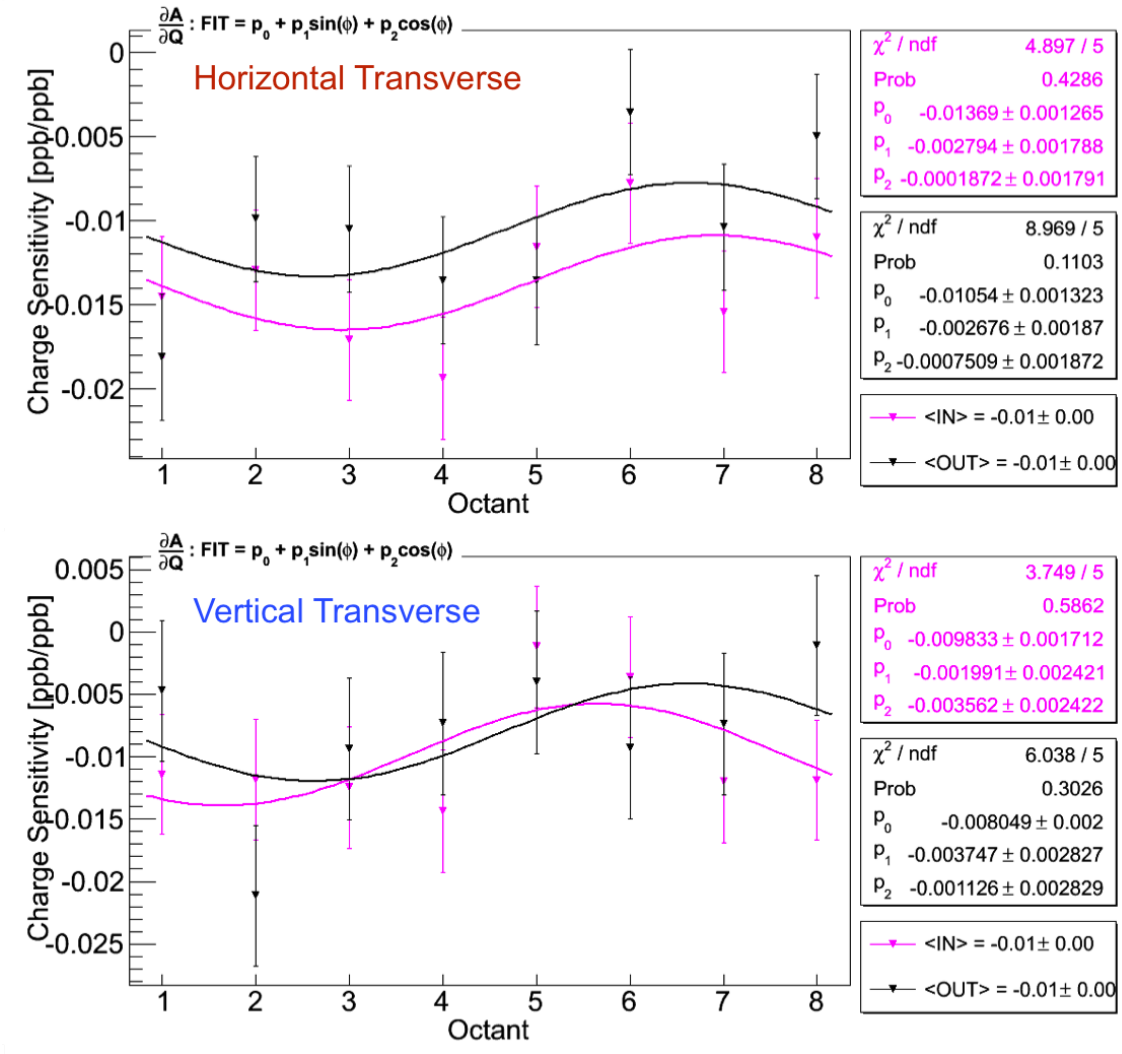

Figure 1.6 Charge sensitivity for horizontal (top) and vertical (bottom) transverse polarization data set. Average charge sensitivities of the measured detector asymmetries extracted from the six parameter (five parameter + charge) regression at beam current 180 μA. Purple (Black) represents the charge sensitivity of the IHWP IN (OUT) data which are consistent with each other. The sensitivities of the eight Čerenkov detectors vary from -0.5% to - 2.0% and are stable within the running period. Average non linearity is -1% for both the cases.

is available. The charge sensitivity of the main detector asymmetries is used as an indicator of the nonlinearity of the system and its contribution is treated as a systematic uncertainty. The nonlinearity term is multiplied with the measured asymmetry to calculate the false asymmetry [6]. The systematic uncertainties due to nonlinearity for horizontal and vertical transverse measurements are given by 0.053 ppm and 0.045 ppm respectively.

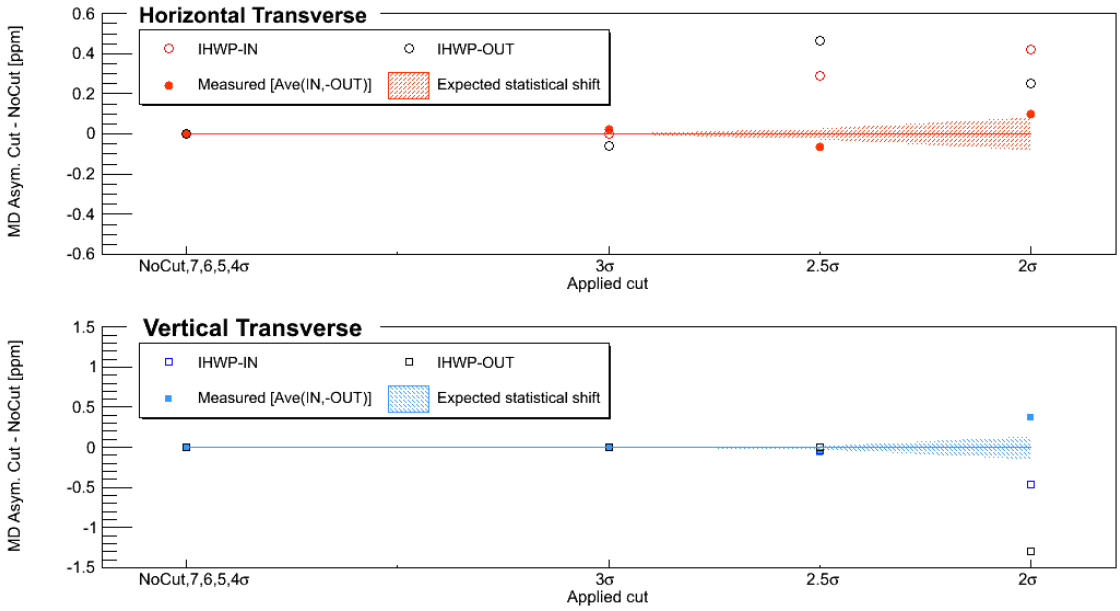

Figure 1.7 Cut dependence study. Shift in the central value of the regressed asymmetry for different cut widths for LH_2. The expected statistical shift is shown by the shaded region using the total number of quartets lost when a cut is applied to all parameters.

1.5.4 Cut Dependence

The goal of the cut dependence analysis was to assign a systematic uncertainty that comes from shifts in the mean value of the regressed asymmetry beyond statistical fluctuations after applied cuts. If linear regression is working properly, large false asymmetries in runlets with large HCBAs should be removed from the measured asymmetry after linear regression is applied and there should not be any shift in the mean value of the regressed asymmetry beyond statistical shifts (as shown in Figure 1.7). The point-to-point uncertainty in going from cut i to cut j is estimated to be

$$\Delta_{i\to j}^{pt-to-pt} = \left(\frac{\sigma_j}{\sqrt{N_j}} - \frac{\sigma_i}{\sqrt{N_i}} \right) \tag{1.5.3}$$

Here the σ is the root mean square (RMS) of each HCBA. Inclusive cuts of 7, 6, 5, 4, 3, 2.5 and 2 σ are applied to all HCBAs and difference between regressed asymmetry with cut and without cuts are shown in Figure 1.7. The observed shift in the measured asymmetry from these cuts are larger than the expected statistical shift and 2.5 σ cuts on the HCBAs were used to assign a systematic uncertainty. The total percentage of quartets lost for cuts with respect to no cut are used to estimate the expected statistical shift, shown as the shaded region in Figure 1.7. Beyond a cut of 2.5 σ, most of the data were removed to extract a meaningful asymmetry. This analysis was performed to assign

systematic uncertainty only, no data was removed from main data set. Cut dependence for horizontal and vertical transverse data set are found to be ∼0.064 ppm and ∼0.068 ppm respectively.

1.5.5 Fit Scheme Dependence

A sinusoidal fit to main detector octant asymmetries is used to extract measured transverse asymmetry. So it was important to find the impact of the function on fitted asymmetry. The measured asymmetry was fitted using four different functions, and the solutions are summarized in Table 1.4. The difference in measured asymmetry obtained using standard function $A_M \sin(\phi + \phi_0) + C$ and rest gives an idea about the fit function dependence of the measured asymmetry. More insightfully, the constant term in the fit function can be thought of as the parity violating asymmetry contribution to the parity conserving transverse asymmetry. The size of transverse asymmetry is much larger than the parity violating asymmetry to have any significant effect on the transverse measurement. So this PV asymmetry is buried under the fit scheme dependence and give rise to the systematic uncertainties of 0.040 ppm for horizontal and 0.083 ppm for vertical transverse data sets.

Table 1.4 Fit scheme dependence of the measured asymmetry. The fit function was varied to observe the effect on measured regressed asymmetry. The difference in asymmetry between case 1 and rest are shown.

	Horizontal transverse			Vertical transverse		
	Fit Function	A_M^H [ppm]	Difference (1-i) [ppm]	Fit Function	A_M^V [ppm]	Difference (1-i) [ppm]
1	$A_M^H \sin(\phi + \phi_0^H) + C^H$	5.343	0.000	$A_M^V \cos(\phi + \phi_0^V) + C^V$	4.525	0.000
2	$A_M^H \sin(\phi + \phi_0^H)$	5.344	0.001	$A_M^V \cos(\phi + \phi_0^V)$	4.510	0.015
3	$A_M^H \sin(\phi) + C^H$	5.303	0.040	$A_M^V \cos(\phi) + C^V$	4.458	0.067
4	$A_M^H \sin(\phi)$	5.304	0.039	$A_M^V \cos(\phi)$	4.442	0.083

1.5.6 Summary of Systematic Uncertainties

Summary of systematic uncertainties of the measured inelastic beam normal single spin asymmetry is given in Table 1.5. The systematic studies contain uncertainties related to the extraction of the measured asymmetry such as regression, nonlinearity, cut dependence, and detector acceptance correction. The systematic studies for horizontal and vertical transverse polarization data set were performed separately; these are summarized in Figure 1.8. Statistical uncertainty weighted average of the systematic uncertainties from horizontal and vertical transverse data sets are considered for the total systematic uncertainty. Total uncertainty is the quadrature sum of the statistical and

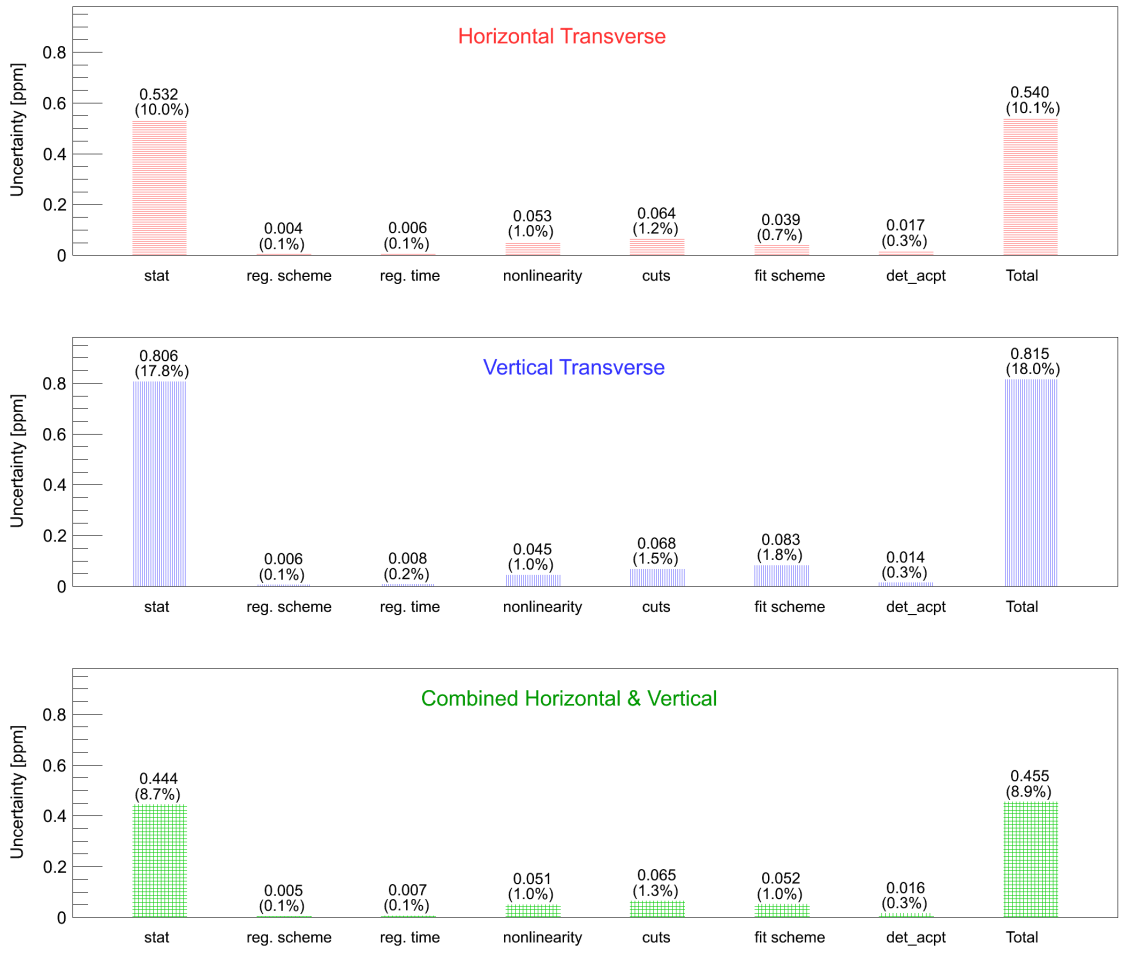

Figure 1.8 Summary of uncertainties on measured asymmetry for horizontal and vertical data set. The relative total uncertainty is dominated by statistical uncertainty compared to systematic uncertainties.

systematic uncertainties. The relative total uncertainty in measured asymmetry is dominated by 9% statistical uncertainty compared to 1% systematic uncertainty.

1.6 Extraction of Physics Asymmetry

The beam normal single spin asymmetry from inelastic e+p scattering is obtained from measured asymmetry using Equation 1.6.1 by accounting for EM radiative corrections, kinematics normalization, polarization, and backgrounds.

$$A_N = R_{total}\left[\frac{\left(\frac{A_M^{in}}{P}\right) - \sum_{i=1}^{4} A_{bi} f_{bi}}{(1 - \sum_{i=1}^{4} f_{bi})}\right] \tag{1.6.1}$$

Table 1.5 Summary of uncertainties on measured asymmetry for combined horizontal and vertical data sets. The relative uncertainties are also shown in the table.

Uncertainty from	Contribution to A_M [ppm]	Relative Contribution [%]
Statistics	0.444	8.7
Regression scheme dependence	0.005	0.1
Regression time dependence	0.007	0.1
Non-linearity	0.051	1.0
Cut dependence	0.065	1.3
Fit scheme dependence	0.052	1.0
Detector acceptance correction	0.016	0.3
Systematic only	0.100	2.0
Total	0.455	8.9

Here R_{total} is a correction factor for the experimental bias and radiative effects, P is the beam polarization, and A_{bi} is i^{th} background asymmetry with fraction of backgrounds in the total detector acceptance (dilution) f_{bi}. The systematic corrections on the physics asymmetry and the associated uncertainties are discussed in the following sections.

1.6.1 Beam Polarization

The Hall-C Møller polarimeter and the Compton polarimeter were used to measure the beam polarization for the experiment, but only the measurements from the Møller polarimeter will be used for this analysis. The photocathode Quantum Efficiency was steady and hence the beam polarization was stable for the period [7]. The Møller polarimeter is only sensitive to longitudinally polarized beam. So measurements performed with the longitudinally polarized beam right after the transverse data taking was used to determine the beam polarization. The Møller runs used for this analysis are 1593 - 1599, carried out on 20th February 2012. Each run is ∼10 min long. Slug averaged polarizations from this Møller measurement are shown in Table 1.6. The measured beam polarization is given by $P = 87.50 \pm 0.28$ (stat) $\pm$ 0.74 (sys)% [8]. Details of systematic studies for the Møller polarization measurement can be found in Q-weak internal technical document [9].

Table 1.6 Beam polarization using Møller polarimeter for Run 2 transverse data set [9].

IHWP	Polarization [%]	Statistical Uncertainty [%]
Out	87.029	0.398
In	- 87.939	0.387
Total	87.497	0.277

1.6.2 Background Corrections

The largest background source in beam normal single spin asymmetry arises from elastic radiative tail. Small background contributions also come from electrons scattering from aluminum target windows, beamline scattering, and other soft neutral scattering. The analysis of the background asymmetries and their contributions to the BNSSA is described in following sections.

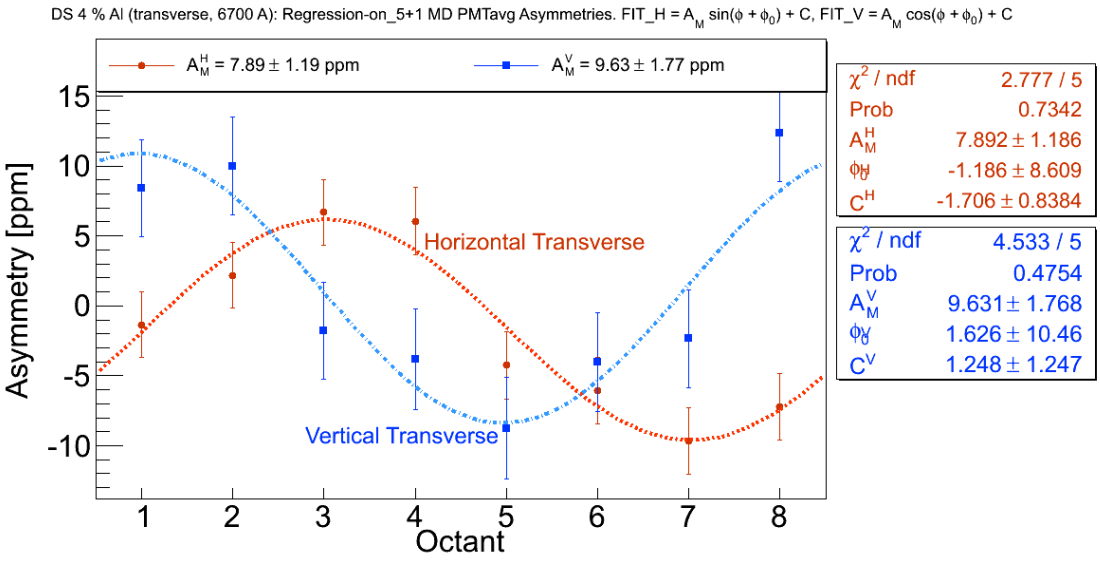

Figure 1.9 Azimuthal dependence of asymmetry from the 4% downstream aluminum target. The uncertainties are statistical only. The octant dependence in either polarization orientation are similar to what was observed for the LH_2-cell. The asymmetry is larger than the LH_2-cell asymmetry. The fit functions used for horizontal and vertical transverse data points are $A_M^H \sin(\phi + \phi_0^H) + C^H$ and $A_M^V \cos(\phi + \phi_0^V) + C^V$ respectively.

1.6.2.1 Target Aluminum Windows

One of the important background contributions to the measured asymmetry comes from electrons scattering from the aluminum alloy target windows. Data were taken on the 4% downstream aluminum alloy target to determine the size of this asymmetry. The measured regressed asymmetry for horizontal and vertical transverse are $A^H_{DSAl} = 7.892 \pm 1.186$ ppm and $A^V_{DSAl} = 9.631 \pm 1.768$ ppm [10], as shown in Figure 1.9. Combined (error weighted) regressed aluminum alloy asymmetry is $A_{DSAl} = 8.432 \pm 0.985$ ppm. This asymmetry is then scaled by a 0.9938 for azimuthal acceptance averaging (already discussed in section 1.4.1), which yields the asymmetry as 8.484±0.985 ppm. The acceptance difference between the upstream and downstream target windows need to correct before the background correction. This acceptance difference causes a 20% relative

difference between the mean Q^2 of the electrons coming from the upstream window compared to the downstream window, as shown in GEANT4 simulations [11] (Q^2_{USAl}=0.8×Q^2_{DSAl}). The beam normal single spin asymmetry from nuclei at forward angle scattering asymmetry is proportional to $\sqrt{Q^2}$ as described in theoretical models [12, 13]. So, asymmetry for upstream aluminum target can be calculated as $A_{USAl} = \sqrt{0.8}A_{DSAl} = 7.589$ ppm. Downstream and upstream aluminum target windows are expected to contribute equally [11] to the aluminum dilution in the main detector asymmetries resulting in an effective aluminum asymmetry of $A_{Al} = (A_{DSAl} + A_{DSAl})/2 = 8.036$ ppm. An additional systematic uncertainty of $0.08 \times A_{Al}$ is assigned for the system non-linearity (more details in APPENDIX **??**). The polarization corrected asymmetry for background windows correction is $A_{b1} = A_{Al}/P = 9.185 \pm 1.409$ ppm. The measured aluminum windows dilution is $f_{b1} = 0.033 \pm 0.002$ [14]. Dedicated measurements were performed with different pressures of hydrogen gas in the target cell. Using the known pressure of hydrogen gas at different points, the pressure was extrapolated to zero. The correction to the physics asymmetry from aluminum alloy windows is $c_{b1} = \kappa P A_{b1} f_{b1} = 1.427$ ppm, where $\kappa = (R_{total}/P)/(1 - f_{total})$.

1.6.2.2 Beamline Scattering

Another correction accounts for scattering sources in the beam line ($b2$), with an asymmetry (A_{b2}) measured, along with its dilution (f_{b2}), by blocking two of the eight openings in the first of the three Pb collimators with tungsten. The measured asymmetry in the blocked octants detectors was correlated with different background detectors located outside the acceptance of the main detectors for scaling during the primary measurement, assuming a constant dilution [15]. The variation of upstream luminosity monitor asymmetry with octant during longitudinal running can provide a good indication of the beamline scattering asymmetry. The maximum variation before and after the transverse data collection period (during longitudinal running) $\Delta A_{\mathrm{USLumi}} = 3.534 \pm 0.16$ ppm was used to estimate the beamline scattering asymmetry. A very simple postulate was considered: that measured main detector asymmetry has a background with a fixed fraction and an asymmetry that scales linearly with that measured in the background monitors and USLumis. The scale factor was measured directly, correlating the MD asymmetry to background asymmetries, and was estimated to be 0.0085 ± 0.0016 [16] from longitudinal period. The signal drops by an order of magnitude lower for inelastic scattering compared to elastic, whereas beamline background remains similar. Hence an additional factor of 10 was multiplied to incorporate the signal drop. The beamline background does not depend on polarization and is not corrected for it. Then, asymmetry for beam line scattering is given by $A_{b2} = \Delta A_{\mathrm{USLumi}} \times 0.085 = 0.300 \pm 0.058$ ppm. The beamline scattering dilution factor

for inelastic running is an order of magnitude larger than in the elastic kinematic setting. The total rate at the inelastic peak drops to 10% of the total rate at the elastic peak, whereas the number of events originating in the beamline remains similar. The measured dilution for inelastic beamline scattering is 0.018 ± 0.001 [17, 18]. A 50% uncertainty on the dilution was assigned to allow the sinusoidal modulation specific to the BNSSA. The beamline scattering dilution used for the background correction is $f_{b2} = 0.018 \pm 0.009$. The correction to the physics asymmetry due to beam line scattering is $c_{b2} = \kappa P A_{b2} f_{b2} = 0.025$ ppm.

1.6.2.3 Other Neutral Background

An additional correction was applied to include soft neutral backgrounds ($b3$) arising from secondary interactions of scattered electrons in the collimators and magnet, and was not accounted in the blocked octant studies [19]. The primary electron interaction at scraping is partially coming from Møller scattering, but the source of the asymmetry is not well understood. The other neutral background asymmetry could be as large as 5 ppm (size of the transverse asymmetry). To make the sign of the asymmetry uncertain, the asymmetry for other neutral background was assumed to be $A_{b3} = 0.000 \pm 10.000$ ppm. Here, uncertainty of 100% of the measured transverse asymmetry was assigned to give an upper bound on the neutral background asymmetry. The neutral background dilution for the inelastic scattering has been measured as $f_{\text{neutral}} = 0.0520 \pm 0.0040$ (stat) ± 0.0014 (sys) [20]. The dilution for the other neutral background was obtained by subtracting the blocked octant background from the total neutral background measured by the main detector and is given by $f_{b3} = f_{\text{neutral}} - f_{b2} = 0.034 \pm 0.010$. The correction to the physics asymmetry due to other neutral background is $c_{b3} = \kappa P A_{b3} f_{b3} = 0.000$ ppm.

1.6.2.4 Elastic Radiative Tail

The largest background correction comes from the elastic radiative tail ($b4$). The polarization corrected measured elastic transverse asymmetry was A_T^{el} = -5.345 ± 0.067 (stat) ± 0.076 (sys) ppm [22]. The elastic physics asymmetry from the LH_2-cell is similar in magnitude to the inelastic asymmetry but has the opposite sign. The elastic asymmetry was measured at $Q^2_{el} = 0.0250 \pm 0.0006$ (GeV/c)^2 [23] where as inelastic measurement was at $Q^2_{in} = 0.0209 \pm 0.0005$ (GeV/c)^2 (shown in Figure 1.12), hence it is necessary to scale it to the inelastic peak. The transverse asymmetry is proportional to $\sqrt{Q^2}$ [12, 13]. The polarization and $\sqrt{Q^2}$ corrected elastic asymmetry is given by $A_{b4} = \sqrt{\frac{Q^2_{in}}{Q^2_{el}}} A_T^{el}$ = -4.885 ± 0.093 ppm. As ∼70% of the total signal in the inelastic peak was from elastic radiative tail (Figure 1.10), it was important to tackle it carefully. A GEANT simulation was used to extract

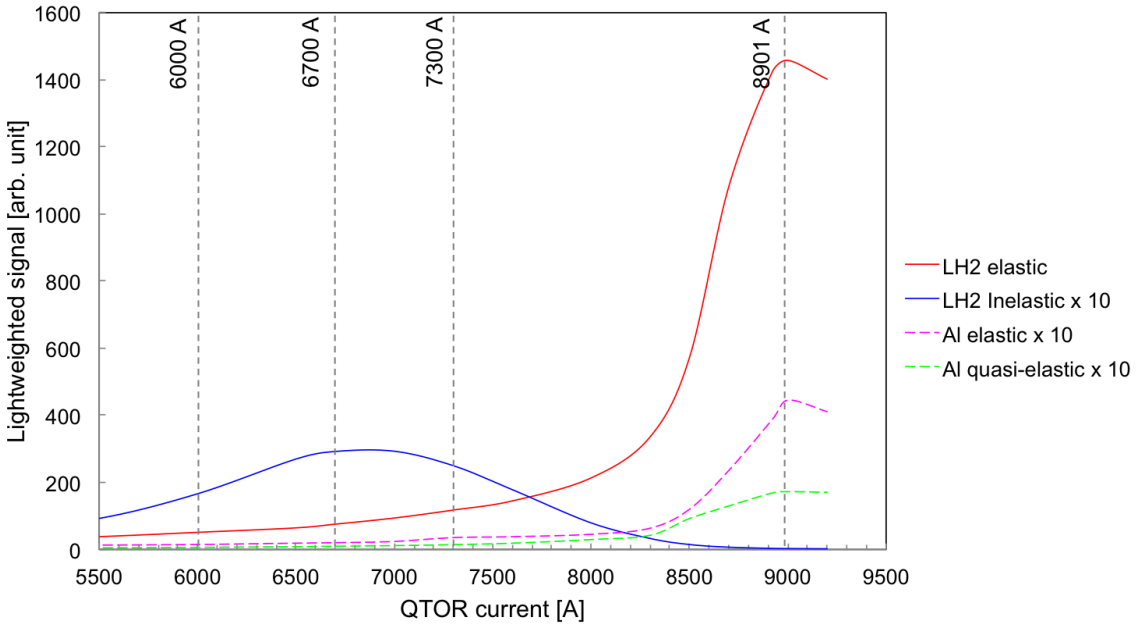

Figure 1.10 Simulation of contributions from elastic and inelastic e+p, and elastic e+Al scattering from upstream (US) and downstream (DS) target windows [21]. All but elastic e+p events have been multiplied by 10 for better visualization.

elastic dilution. Dedicated measurements were taken at both sides of the inelastic peak (at QTor current 6000 A and 7300 A) to verify the simulation. A ∼10% discrepancy was observed between current mode data and GEANT simulated signal at the inelastic peak, as shown in Figure 1.11. In order to incorporate this discrepancy, a 10% systematic uncertainty was assigned to the elastic dilution for this preliminary analysis. A more detailed simulation is ongoing to explore this difference. The signal size for inelastic transverse is ∼2-3 times smaller than that of the elastic signal. Although the signal reduces for inelastic, the nonlinearity in the detector remains the same and might be responsible for this discrepancy. The simulated elastic dilution factor is given by $f_{b4} = 0.701 \pm 0.070$ [21, 24]. The correction to the physics asymmetry due to the elastic radiative tail is $c_{b4} = \kappa P A_{b4} f_{b4}$ = -16.129 ppm.

1.6.3 Other Corrections

Another set of corrections is used to remove all the experimental bias from the measured asymmetry before extracting BNSSA. The measured asymmetry is corrected for the electromagnetic (EM) radiative corrections, light weighting on the Čerenkov detector, and Q^2 precision. These corrections are considered as independent factors and are applied to the measured asymmetry.

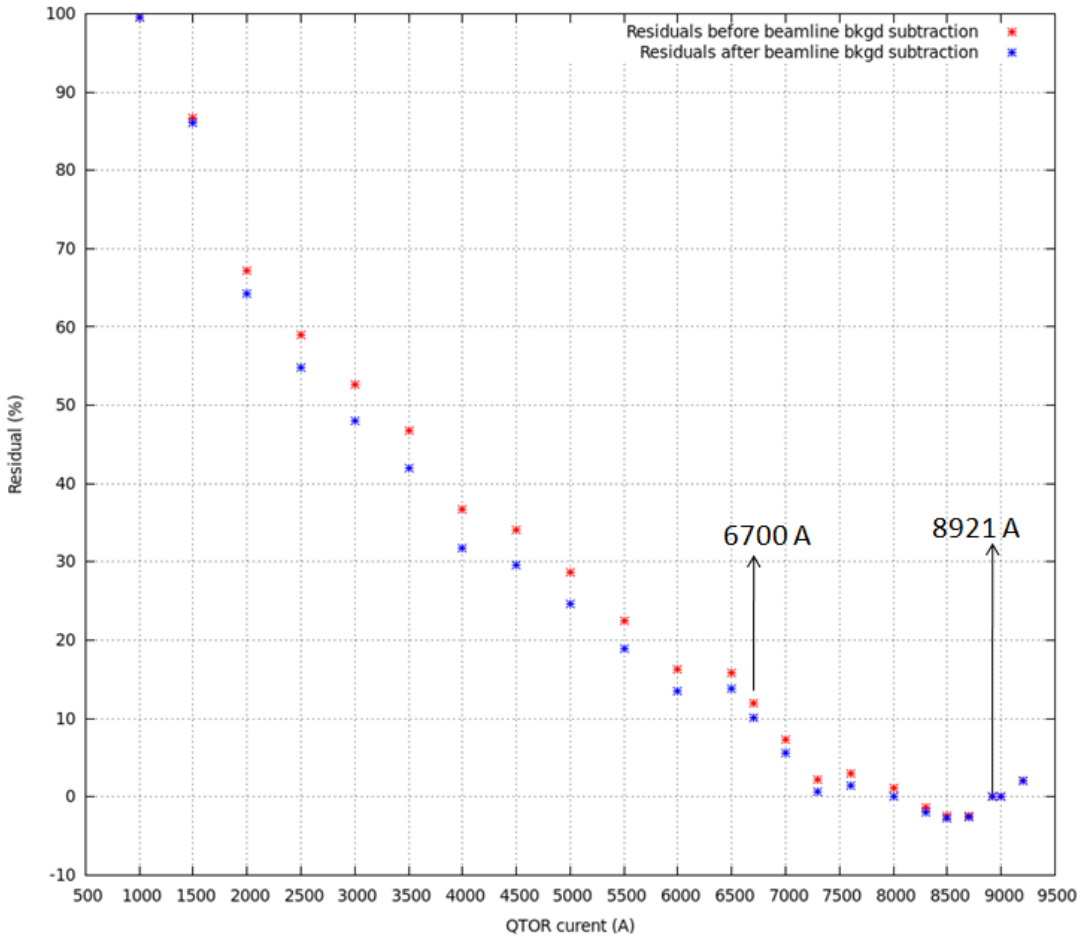

Figure 1.11 The residual of yield using Data and simulation from GEANT 3 [21] are shown in the figure. A ∼10% discrepancy was observed at inelastic peak (6700 A) between data and simulation for matching them at elastic peak (8921 A). Beamline background correction to the yield did not improve the discrepancy.

1.6.3.1 Radiative Correction

The energy loss and depolarization of the electrons is a result of electromagnetic (EM) radiation [25]. The measured asymmetry needs to be corrected for these EM radiative effects to obtain the beam normal single spin asymmetry at the effective Q^2 and beam polarization. The deduced radiative correction for elastic e+p scattering from simulations with and without bremsstrahlung, using methods described in Refs. [26, 27], was found to be $R_{RC} = 1.010 \pm 0.004$ [28]. The same radiative correction was used for this data set as there were no existing simulations available for inelastic e+p scattering. This correction does not have a significant impact in the final asymmetry, hence it was not unreasonable to use the existing elastic simulation result.

1.6.3.2 Detector Bias Correction

The measured light variation and nonuniform Q^2 distribution across the detector bars affects the measured asymmetry and need to be accounted for in the final BNSSA extraction.

$$R_{Det} = \frac{A^{\text{sim}}_{\text{no-bias}}}{A^{\text{sim}}_{\text{bias}}} = \sqrt{\frac{(Q^2)^{\text{sim}}_{\text{no-bias}}}{(Q^2)^{\text{sim}}_{\text{bias}}}} \tag{1.6.2}$$

Here, $A^{\text{sim}}_{\text{bias}}$ and $A^{\text{sim}}_{\text{no-bias}}$ are the simulated asymmetries with and without light-collection bias respectively. The detector bias correction used for this analysis is $R_{Det} = 0.998 \pm 0.001$ and is obtained using elastic transverse simulation results [28, 29].

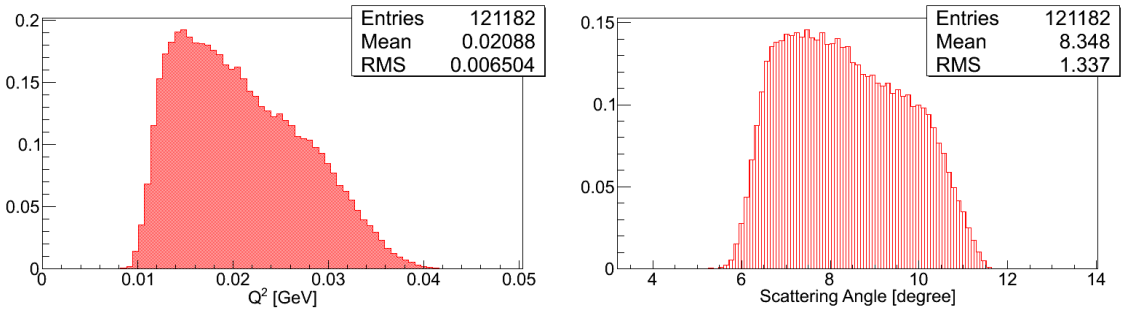

Figure 1.12 The Q^2 from GEANT 3 simulation [30]. The Q^2 was weighted by cross section and did not include any internal bremsstrahlung in the simulation (left panel). The simulated scattering angle is also shown in the right panel.

1.6.3.3 Q^2 Precision

The Q^2 for inelastic e+p scattering was determined using GEANT 3 simulation and was found to be 0.0209 ± 0.0005 $(GeV/c)^2$ [30], as shown in Figure 1.12. Internal bremsstrahlung was not included in the simulation. The simulation was benchmarked by the tracking mode experimental data to represent the geometry of the experimental setup, collimation, and magnetic spectrometer. The cross section weighted Q^2 was simulated at main detector using the reaction $e+p \rightarrow e+n+\pi^+$. The two-body scattering process, and energy and momentum conservation were used to do the calculation. The scattered electron energy, and Q^2 are expressed as

$$\begin{aligned} E' &= RANDOM() \times (E_{in} - M_e) + M_e \\ Q^2 &= 4EE'sin^2\theta, \end{aligned} \tag{1.6.3}$$

where E_{in} is the incident beam, M_e is electron mass, and θ is scattering angle. A 2.0% run to run variation of Q^2 was seen from the tracking data and added as systematic uncertainty in Q^2 estimation. It was important to propagate the precision of Q^2 in the final physics asymmetry. Based on theory [31], the transverse beam spin asymmetries A_N at low Q^2 behave like

$$A_N \approx \sqrt{Q^2} = m\sqrt{Q^2}. \tag{1.6.4}$$

$$dA_N = \pm\frac{1}{2}\frac{m}{\sqrt{Q^2}}dQ^2 = \pm\frac{1}{2}\frac{34.7}{\sqrt{0.02078}}0.0005 = 0.0601ppm \tag{1.6.5}$$

Using Equation 1.6.4 on Q^2 and a 5 ppm measured asymmetry, the proportionality constant in the above relation can be calculated as 34.7 ppm/(GeV/c). The estimated uncertainty on the measured asymmetry due to the uncertainty in determining Q^2 is 0.061 ppm (Equation 1.6.5). A correction of $R_{Q^2} = 1.000 \pm 0.012$ was applied to include the precision in calibrating the central value of Q^2.

1.6.4 Beam Normal Single Spin Asymmetry

Summary of required quantities to extract the beam normal single spin asymmetry from the transverse data set presented so far using

$$A_N = R_{RC}R_{Det}R_{Q^2}R_{\phi}\left[\frac{\left(\frac{A_M^{in}}{P}\right) - A_{b1}f_{b1} - A_{b2}f_{b2} - A_{b3}f_{b3} - A_{b4}f_{b4}}{1 - f_{b1} - f_{b2} - f_{b3} - f_{b4}}\right] \tag{1.6.6}$$

is shown in Table 1.7. Equation 1.6.1 has been expanded to obtain Equation 1.6.6. Using all the input values in Equation 1.6.6 gives the beam normal single spin asymmetry in inelastic e+p scattering

$$A_N = 42.27 \pm 2.45 \text{ (stat)} \pm 15.73 \text{ (sys) ppm} \tag{1.6.7}$$

for the effective kinematics of acceptance averaged electron energy $\langle E\rangle = 1.155 \pm 0.003$ GeV, $\langle Q^2\rangle = 0.0209 \pm 0.0005$ (GeV/c)^2 and an average scattering angle $\langle\theta\rangle = 8.3 \pm 1.3°$. The contributions from the different uncertainty sources into the final measurement are summarized in Figure 1.13. The dominant correction to the asymmetry comes from the elastic dilution tail whereas the dominant uncertainty on the measured asymmetry comes from statistics.

Table 1.7 Summary of input quantities to extract BNSSA. The measured regressed asymmetry is corrected for detector acceptance using the factor provided in the table. The table shows the contributions of normalization factors on A_M^{in}, then the properly normalized contributions from other sources. Background corrections listed here include only $R_{\text{total}} f_i A_i/(1-f_{total})$. Uncertainties in BNSSA due to dilution fraction and background asymmetry uncertainties are noted separately.

Input parameters			
Measured asymmetry (A_M^{in})	5.095 ± 0.455 ppm		
Beam polarization (P)	0.875 ± 0.008		
Detector acceptance correction	0.9938		
Background corrections			
Quantity	Asymmetry (A_{bi}) [ppm]	Dilution (f_{bi})	Correction $c_i = \kappa P A_{bi} f_{bi}$ [ppm]
Target windows (b1)	9.185 ± 1.409	0.033 ± 0.002	1.427
Beamline scattering (b2)	0.300 ± 0.058	0.018 ± 0.009	0.025
Other neutral bkg. (b3)	0.000 ± 10.000	0.034 ± 0.010	0.000
Elastic asymmetry (b4)	-4.885 ± 0.093	0.701 ± 0.070	-16.129
Other corrections			
Radiative correction (R_{RC})	1.010 ± 0.004		
Detector bias (R_{Det})	0.998 ± 0.001		
Q^2 acceptance (R_{Q^2})	1.000 ± 0.012		

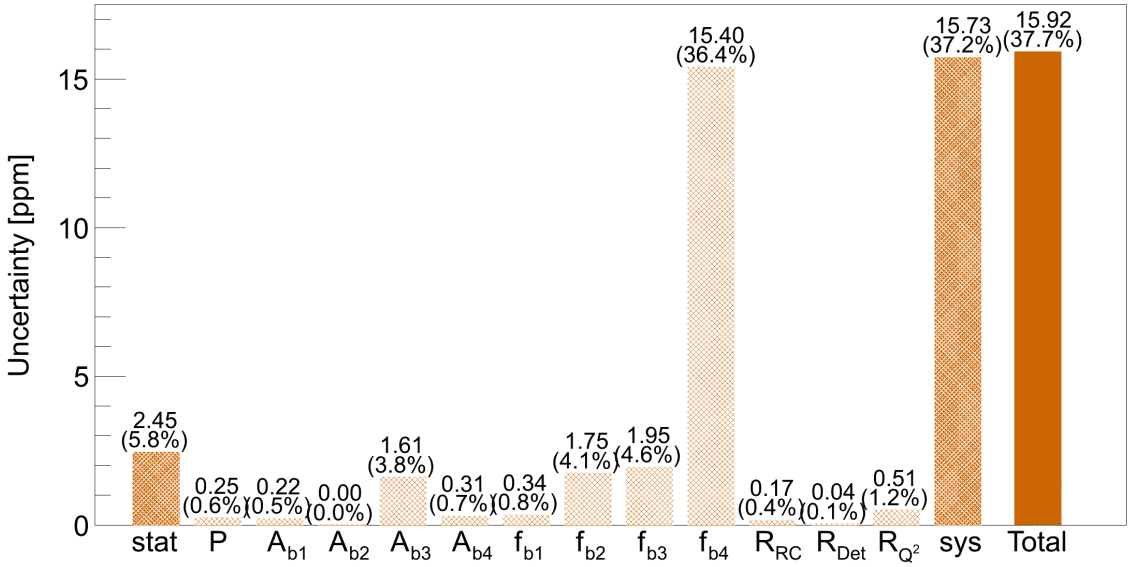

Figure 1.13 Summary of uncertainties in inelastic beam normal single spin asymmetry extraction. Measurement systematic contains the systematic uncertainties related to the extraction of the physics asymmetry such as regression, nonlinearity and acceptance averaging. The uncertainties are in ppm and the corresponding relative uncertainties are shown in parentheses.

1.7 Comparison With Model Calculation

No existing model calculation for beam normal single spin asymmetry was available at Q-weak kinematics during this analysis. Pasquini et al. [32] presented beam asymmetry in inelastic electron scattering (as shown in Figure **??**) for large scattering angle at energies E = 0.424, 0.570, 0.855 GeV. The BNSSA were calculated separately for Δ and N intermediate states. Total asymmetry was the sum of these two intermediate states. Large asymmetries were observed in the forward region; these are dominated by quasi Virtual Compton Scattering (VCS) kinematics where one exchanged photon becomes quasi-real. These asymmetries are sensitive to $\gamma^*\Delta\Delta$ form factors and can be a unique tool to study it [33].

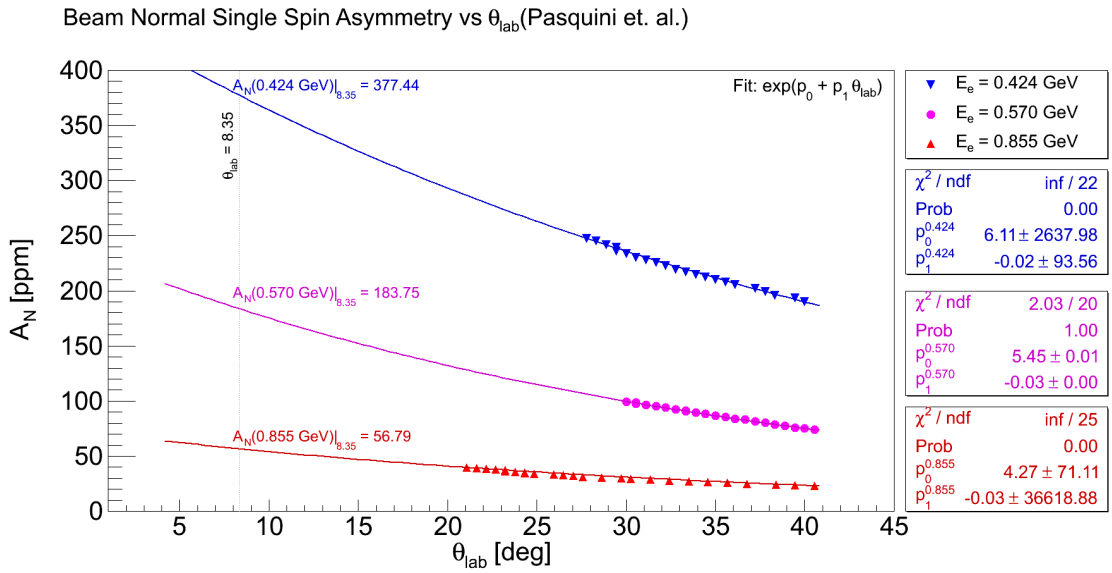

Figure 1.14 BNSSA asymmetry calculation from Pasquini et al. The points are taken from [32]. Then, the calculation is fitted with a function of the form $f(\theta_{\rm lab}) = exp(p_0 + p_1\theta_{\rm lab})$ and interpolated to Q-weak $\theta_{\rm lab}$ value.

These asymmetries were interpolated to forward angle up to $\theta_{\rm lab}$<5° using a suitable fit for all available three energies from [32], as shown in Figure 1.14. The asymmetries were obtained at $\theta_{\rm lab}$ = 8.35° for three energies and extrapolated to Q-weak energy E = 1.155 GeV in Figure 1.15. Using this hand waving toy model, the obtained BNSSA is A_N[model] = 12.15 ppm at Q-weak kinematics. The asymmetry from this analysis, A_N[Q-weak] = 42.27 ± 15.92 ppm is also shown in the Figure 1.15.

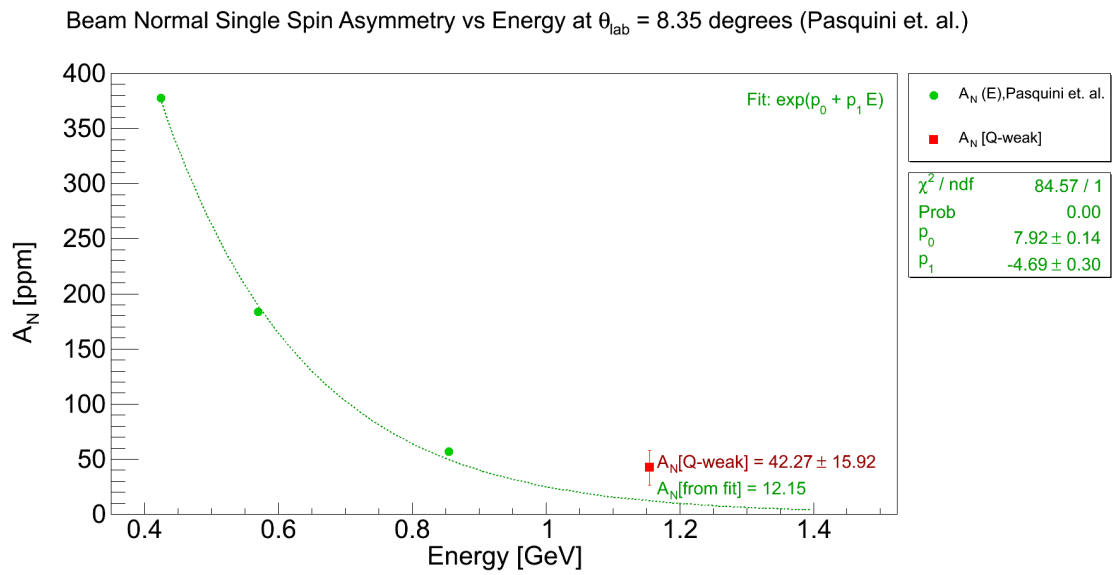

Figure 1.15 BNSSA asymmetry calculation from Pasquini et al. and its extension. The asymmetries from Figure 1.14 at $\theta_{\rm lab} = 8.35°$ are plotted here. A fit function of the form $f(E) = exp(p_0 + p_1 E)$ is used to extrapolate the asymmetry to the desired Q-weak kinematic region ($E = 1.155$ GeV).

1.8 BNSSA in Nuclear Targets

In this chapter, the inelastic beam normal single spin asymmetry measurements in e-p scattering have been discussed. In addition to the inelastic data from the proton, Q-weak has data on the beam normal single spin asymmetry measurements from several other physics processes. Few of these measurements are the first of their kind and carry interesting physics. The measured regressed (5+1) asymmetries on liquid hydrogen cell, 4% thick downstream aluminum alloy, and a 1.6% thick downstream carbon foil are summarized in Table 1.8. The relative statistical precision of the measurements are also shown in the Table. The analysis of these data is ongoing and expected to test model calculations of beam normal single spin asymmetry.

1.9 Conclusion

The Q-weak collaboration has made a 35% relative measurement of the beam normal single spin asymmetry of $A_N = 42.27 \pm 2.45$ (stat) $\pm$ 15.73 (sys) ppm using transversely polarized 1.155 GeV electrons scattering in-elastically from protons with a Q^2 of 0.0209 (GeV/c)^2. This is the first measurement of the beam normal single spin asymmetry in inelastic e-p scattering. This measurement

Table 1.8 Measured regressed (5+1) asymmetries in inelastic electron-nucleon scattering for transverse polarized beam. Horizontal and vertical transverse data set are shown separately. The combined (error weighted average) asymmetries are also noted. The inelastic peak is at QTor current 6700 A. The other QTor currents were taken to improve the simulation for elastic radiative tail.

Pol.	Asymmetry [ppm]					
	QTor currents					
	6000 A	6700 A			7300 A	
	LH_2	$LH_2^{\dagger}$	$Al^{\dagger\dagger}$	^{12}C	LH_2	Al
Hor.	7.212±0.688	5.343±0.532	7.892±1.186	10.190±1.863	0.967±0.477	-1.245±1.087
Ver.		4.525±0.806	9.631±1.768			
Com.	7.212±0.688	5.095±0.444	8.432±0.985	10.190±1.863	0.967±0.477	-1.245±1.087
	(9.5%)	(8.7%)	(11.7%)	(18.3%)	(49.3%)	(87.3%)

would be an excellent test of theoretical calculations. Unfortunately, at the time of this analysis, there was no existing theoretical calculation or model to compare with the data. Hopefully this thesis will encourage theoreticians to produce new calculations.

REFERENCES

[1] Q weak Collaboration. The Q-weak Experiment: "A Search for New Physics at the TeV Scale via a Measurement of the Proton's Weak Charge". Technical Report E05-008 Jeopardy proposal, December 2007. (Cited on page 1.)

[2] P. Pébay. Formulas for robust, One-Pass Parallel Computation of Covariances and Arbitrary-Order Statistical Moments. Sandia Report SAND2008-6212, Sandia National Laboratories, 2008. (Cited on page 4.)

[3] Jim Birchall. Effect of averaging over azimuthal angle. ELOG-Analysis-373: https://qweak.jlab.org/elog/Analysis+&+Simulation/373, June 2011. (Cited on page 8.)

[4] Rakitha Beminiwattha. *A Measurement of the Weak Charge of the Proton through Parity Violating Electron Scattering using the Qweak Apparatus: A 21% Result.* PhD thesis, Ohio University, Athens OH 45701, USA, August 2013. (Cited on page 9.)

[5] Dave Mack. BCM Normalization Issues Part II: Calibrations and Linearity. Q-weak-DocDB1369: https://qweak.jlab.org/doc-private/ShowDocument?docid=1369, March 2011. (Cited on page 10.)

[6] Dave Mack. Non-linearity Specification for the Qweak Detector Chain. Technical Report Qweak-DocDB-172, November 2004. (Cited on page 11.)

[7] Joshua Magee. Private communication, 2014. (Cited on page 15.)

[8] Nuruzzaman. Beam Polarization from Moller Polarimeter for Transverse Run-II Dataset. ELOG-Ancillary-91: https://qweak.jlab.org/elog/Ancillary/91, April 2014. (Cited on page 15.)

[9] Joshua Magee. The Qweak Run 2 Moller Polarimetry Analysis. Technical Report Qweak-DocDB-1955, January 2014. (Cited on page 15.)

[10] Nuruzzaman. Transverse Asymmetries for N-to-Delta in Nuclear Targets. ELOG-Ancillary-43: https://qweak.jlab.org/elog/Ancillary/43, July 2013. (Cited on page 16.)

[11] Kathrine Myers. *The First Determination of the Proton's Weak Charge Through Parity-Violating Asymmetry Measurements in Elastic e+p and e+Al Scattering.* PhD thesis, The George Washington University, Washington, DC 20052, USA, May 2012. (Cited on page 17.)

[12] E. D. Cooper and C. J. Horowitz. Vector analyzing power in elastic electron-nucleus scattering. *Phys. Rev. C*, 72:034602, Sep 2005. (Cited on pages 17 and 18.)

[13] M. Gorchtein and C. J. Horowitz. Analyzing power in elastic scattering of electrons off a spin-0 target. *Phys. Rev. C*, 77:044606, Apr 2008. (Cited on pages 17 and 18.)

[14] Josh Magee. Aluminum Status Qweak Collaboration Meeting. Hall C collaboration meeting, Q-weak-DocDB1891: https://qweak.jlab.org/doc-private/ShowDocument?docid=1819, April 2013. (Cited on page 17.)

[15] Kent Paschke. Proposed Wien0 neutral beamline background correction. ELOG-Analysis-782: https://qweak.jlab.org/elog/Analysis+&+Simulation/782, October 2012. (Cited on page 17.)

[16] Manolis Kargiantoulakis. Beamline Backgrounds Update. ELOG-Analysis-1191: https://qweak.jlab.org/elog/Analysis+&+Simulation/1191, July 2014. (Cited on page 17.)

[17] John Leacock. *Measuring the Weak Charge of the Proton and the Hadronic Parity Violation of the $N \rightarrow \Delta$ Transition*. PhD thesis, Virginia Polytechnic Institute & State University, Blacksburg, VA 24061-0002, USA, October 2012. (Cited on page 18.)

[18] Dave Mack. Wien0 Beamline Background Dilution Central Value and Uncertainty. ELOG-Analysis-784: https://qweak.jlab.org/elog/Analysis+&+Simulation/784, October 2012. (Cited on page 18.)

[19] Dave Mack. Input file for Wien 0 elastic e+p asymmetry corrections (v11 frozen modulo unblinding). ELOG-Analysis-714: https://qweak.jlab.org/elog/Analysis+&+Simulation/714, September 2012. (Cited on page 18.)

[20] Rakitha S Beminiwattha. Main Detector Neutral Background Contribution. Technical Report Qweak-DocDB-1549, July 2012. (Cited on page 18.)

[21] Adesh Subedi. Simulation of QTor scans using QWGEANT3. ELOG-Analysis-837: https://qweak.jlab.org/elog/Analysis+&+Simulation/837, December 2012. (Cited on pages 19 and 20.)

[22] Buddhini Waidyawansa. Qweak Transverse Asymmetry Measurements. Hall C collaboration meeting, Q-weak-DocDB1961: https://qweak.jlab.org/doc-private/ShowDocument?docid=1961, February 2014. (Cited on page 18.)

[23] D. Androic, D. S. Armstrong, A. Asaturyan, T. Averett, J. Balewski, J. Beaufait, R. S. Beminiwattha, J. Benesch, F. Benmokhtar, J. Birchall, R. D. Carlini, G. D. Cates, J. C. Cornejo, S. Covrig, M. M. Dalton, C. A. Davis, W. Deconinck, J. Diefenbach, J. F. Dowd, J. A. Dunne, D. Dutta, W. S. Duvall, M. Elaasar, W. R. Falk, J. M. Finn, T. Forest, D. Gaskell, M. T. W. Gericke, J. Grames, V. M. Gray, K. Grimm, F. Guo, J. R. Hoskins, K. Johnston, D. Jones, M. Jones, R. Jones, M. Kargiantoulakis, P. M. King, E. Korkmaz, S. Kowalski, J. Leacock, J. Leckey, A. R. Lee, J. H. Lee, L. Lee, S. MacEwan, D. Mack, J. A. Magee, R. Mahurin, J. Mammei, J. W. Martin, M. J. McHugh, D. Meekins, J. Mei, R. Michaels, A. Micherdzinska, A. Mkrtchyan, H. Mkrtchyan, N. Morgan, K. E. Myers, A. Narayan, L. Z. Ndukum, V. Nelyubin, Nuruzzaman, W. T. H. van Oers, A. K. Opper, S. A. Page, J. Pan, K. D. Paschke, S. K. Phillips, M. L. Pitt, M. Poelker, J. F. Rajotte, W. D. Ramsay, J. Roche, B. Sawatzky, T. Seva, M. H. Shabestari, R. Silwal, N. Simicevic, G. R. Smith, P. Solvignon, D. T. Spayde, A. Subedi, R. Subedi, R. Suleiman, V. Tadevosyan, W. A. Tobias, V. Tvaskis, B. Waidyawansa, P. Wang, S. P. Wells, S. A. Wood, S. Yang, R. D. Young, and S. Zhamkochyan. First determination of the weak charge of the proton. *Phys. Rev. Lett.*, 111:141803, Oct 2013. (Cited on page 18.)

[24] Nuruzzaman. Comparison of H2 Dilutions from Geant-III, IV, and Data at the Inelastic Peak. ELOG-Ancillary-59: https://qweak.jlab.org/elog/Ancillary/59, December 2013. (Cited on page 19.)

[25] Haakon Olsen and L. C. Maximon. Photon and electron polarization in high-energy bremsstrahlung and pair production with screening. *Phys. Rev.*, 114:887–904, May 1959. (Cited on page 20.)

[26] K. A. Aniol, D. S. Armstrong, M. Baylac, E. Burtin, J. Calarco, G. D. Cates, C. Cavata, J.-P. Chen, E. Chudakov, D. Dale, C. W. de Jager, A. Deur, P. Djawotho, M. B. Epstein, S. Escoffier, L. Ewell, N. Falletto, J. M. Finn, K. Fissum, A. Fleck, B. Frois, J. Gao, F. Garibaldi, A. Gasparian, G. M. Gerstner, R. Gilman, A. Glamazdin, J. Gomez, V. Gorbenko, O. Hansen, F. Hersman, R. Holmes, M. Holtrop, B. Humensky, S. Incerti, J. Jardillier, M. K. Jones, J. Jorda, C. Jutier, W. Kahl, D. H. Kim, M. S. Kim, K. Kramer, K. S. Kumar, M. Kuss, J. LeRose, M. Leuschner, D. Lhuillier, N. Liyanage, R. Lourie, R. Madey, D. J. Margaziotis, F. Marie, J. Martino, P. Mastromarino, K. McCormick, J. McIntyre, Z.-E. Meziani, R. Michaels, G. W. Miller, D. Neyret, C. Perdrisat, G. G. Petratos, R. Pomatsalyuk, J. S. Price, D. Prout, V. Punjabi, T. Pussieux, G. Quéméner, G. Rutledge, P. M. Rutt, A. Saha, P. A. Souder, M. Spradlin, R. Suleiman, J. Thompson, L. Todor, P. E. Ulmer, B. Vlahovic, K. Wijesooriya,

R. Wilson, and B. Wojtsekhowski. Measurement of the neutral weak form factors of the proton. *Phys. Rev. Lett.*, 82:1096–1100, Feb 1999. (Cited on page 20.)

[27] K. A. Aniol, D. S. Armstrong, T. Averett, M. Baylac, E. Burtin, J. Calarco, G. D. Cates, C. Cavata, Z. Chai, C. C. Chang, J.-P. Chen, E. Chudakov, E. Cisbani, M. Coman, D. Dale, A. Deur, P. Djawotho, M. B. Epstein, S. Escoffier, L. Ewell, N. Falletto, J. M. Finn, K. Fissum, A. Fleck, B. Frois, S. Frullani, J. Gao, F. Garibaldi, A. Gasparian, G. M. Gerstner, R. Gilman, A. Glamazdin, J. Gomez, V. Gorbenko, O. Hansen, F. Hersman, D. W. Higinbotham, R. Holmes, M. Holtrop, T. B. Humensky, S. Incerti, M. Iodice, C. W. de Jager, J. Jardillier, X. Jiang, M. K. Jones, J. Jorda, C. Jutier, W. Kahl, J. J. Kelly, D. H. Kim, M.-J. Kim, M. S. Kim, I. Kominis, E. Kooijman, K. Kramer, K. S. Kumar, M. Kuss, J. LeRose, R. De Leo, M. Leuschner, D. Lhuillier, M. Liang, N. Liyanage, R. Lourie, R. Madey, S. Malov, D. J. Margaziotis, F. Marie, P. Markowitz, J. Martino, P. Mastromarino, K. McCormick, J. McIntyre, Z.-E. Meziani, R. Michaels, B. Milbrath, G. W. Miller, J. Mitchell, L. Morand, D. Neyret, C. Pedrisat, G. G. Petratos, R. Pomatsalyuk, J. S. Price, D. Prout, V. Punjabi, T. Pussieux, G. Quéméner, R. D. Ransome, D. Relyea, Y. Roblin, J. Roche, G. A. Rutledge, P. M. Rutt, M. Rvachev, F. Sabatie, A. Saha, P. A. Souder, M. Spradlin, S. Strauch, R. Suleiman, J. Templon, T. Teresawa, J. Thompson, R. Tieulent, L. Todor, B. T. Tonguc, P. E. Ulmer, G. M. Urciuoli, B. Vlahovic, K. Wijesooriya, R. Wilson, B. Wojtsekhowski, R. Woo, W. Xu, I. Younus, and C. Zhang. Parity-violating electroweak asymmetry in $\vec{e}p$ scattering. *Phys. Rev. C*, 69:065501, Jun 2004. (Cited on page 20.)

[28] Buddhini Waidyawansa. *A 3% Measurement of the Beam Normal Single Spin Asymmetry in Forward Angle Elastic Electron-Proton Scattering using the Qweak Setup*. PhD thesis, Ohio University, Athens OH 45701, USA, August 2013. (Cited on pages 20 and 21.)

[29] Peiqing Wang. Simulated octant-by-octant event rate, scattering angle and momentum transfer. ELOG-Analysis-589: https://qweak.jlab.org/elog/Analysis+&+Simulation/589, May 2012. (Cited on page 21.)

[30] Nuruzzaman. Q^2 for transverse N-to-Delta from GEANT-III. ELOG-Ancillary-44: https://qweak.jlab.org/elog/Ancillary/44, July 2013. (Cited on page 21.)

[31] Andrei V. Afanasev and N.P. Merenkov. Collinear photon exchange in the beam normal polarization asymmetry of elastic electron?proton scattering. *Physics Letters B*, 599(1?2):48 – 54, 2004. (Cited on page 22.)

[32] Barbara Pasquini. Two-Photon Physics: Theory. MAMI and Beyond: http://wwwkph.kph.uni-mainz.de/T//MAMIandBeyond/02%20Dienstag/08%20Pasquini.pdf, April 2009. (Cited on page 24.)

[33] Constantia Alexandrou, Tomasz Korzec, Giannis Koutsou, Cdric Lorc, John W. Negele, Vladimir Pascalutsa, Antonios Tsapalis, and Marc Vanderhaeghen. Quark transverse charge densities in the from lattice {QCD}. *Nuclear Physics A*, 825(1?2):115 – 144, 2009. (Cited on page 24.)